Rapid Characterisation of Protein Phase Behaviour Using Droplet Microfluidics

William E. Arter,[†,¶] Runzhang Qi,[†,¶] Georg Krainer,[†,¶] Timothy Welsh,[†] Yufan Xu,[†]

Peter St George-Hyslop,[$] Simon Alberti[#] and Tuomas P.J. Knowles[‡,*]

[†] Department of Chemistry, University of Cambridge,

Lensfield Road, Cambridge CB2 1EW, UK

[‡] Cavendish Laboratory, Department of Physics, University of Cambridge,

J J Thomson Ave, Cambridge CB3 0HE, UK

[$]Cambridge Institute for Medical Research, Department of Clinical Neurosciences,

University of Cambridge, Cambridge CB2 0XY, UK; Department of Medicine (Division of

Neurology), University of Toronto and University Health Network, Toronto,

Ontario M5S 3H2, Canada

[#] Biotechnology Center (BIOTEC), Center for Molecular and Cellular Bioengineering

(CMCB), Technische Universität Dresden, Tatzberg 47/49, 01307 Dresden, Germany

[¶] These authors contributed equally

* To whom correspondence should be addressed:

E-mail: tpjk2@cam.ac.uk

Abstract

The assembly of intracellular proteins into biomolecular condensates via liquid–liquid phase separation (LLPS) has emerged as a fundamental process underlying the organisation and regulation of cellular space and function. Physicochemical characterisation of the parameters that control and modulate phase separation is therefore essential for an improved understanding of protein phase behaviour, not least to inform efforts for the therapeutic modulation of LLPS phenomena. Given the rapidly increasing number of biologically and disease-relevant condensate systems, experimental techniques that enable high-throughput analysis of protein phase behaviour are required. Here, we present a droplet microfluidic platform, termed PhaseScan, for the rapid generation of protein phase diagrams, a fundamental measure with which to characterise protein phase behaviour in chemical space. Using this platform, we demonstrate characterisation of the phase behaviour of a pathologically relevant mutant of the protein fused in sarcoma (FUS) in a highly parallelised manner, with significantly improved assay throughout and reduced sample consumption with respect to conventional experiments. We find that the phase boundary at which FUS transitions from a one-phase to a two-phase state is modulated by the small molecule 1,6-hexanediol, and estimate the free-energy landscape of this system using Flory–Huggins theory. Our study thus provides a basis for the rapid acquisition of phase diagrams through the application of microdroplet techniques and paves the way for a wide range of applications, enabling swift characterisation of the effect of environmental conditions and coacervate species on the thermodynamics of phase separation.

Introduction

Many cellular proteins have the ability to demix spontaneously into a protein-rich liquid condensate phase and a protein-depleted diluted phase.[1] This process, known as liquid–liquid phase separation (LLPS), has emerged as a fundamental mechanism to describe the organisation of biological matter in living cells.[2] Condensates formed thorough LLPS compartmentalise cellular space,[3] act as microreactors for biochemical reactions,[4] and are crucial to a wide range of physiological processes.[5–7] Phase separating proteins are heavily implicated in protein misfolding diseases including motor neuron disease[8,9] as well as cancer pathogenesis,[10] thus making them an attractive target for therapeutic intervention.[11,12]

Phase separation, now established for hundreds of cellular proteins,[13] can be triggered by minute variations in environmental conditions such as changes in ionic strength, pH, temperature, molecular crowding, and the presence of small molecules.[14–17] Because of this sensitivity to physicochemical parameters, many phase separating protein systems are currently receiving intense interest as fundamentally novel drug targets to ameliorate human diseases.[18,19] However, there is currently an unmet need to quantify the physical parameters that modulate phase separation behaviour in LLPS systems with high fidelity and accuracy.[14]

A fundamental measure with which to describe the thermodynamics of condensate systems is the phase diagram (Figure 1).[19–21] Phase diagrams powerfully summarise the phase-behaviour of LLPS systems by monitoring the position of the chemical equilibrium between the phase-separated and the mixed regimes through determination of the position of the phase boundary in chemical space. Changes in the phase boundary for an LLPS system following variation of solution conditions affords insights to the thermodynamic processes driving protein condensation and the factors that modulate them.[15] As such, the generation of phase diagrams is a vital step to an understanding of protein phase-separation behaviour.

However, given the large variety of proteins undergoing LLPS and the environmental conditions which regulate their behaviour, there is a need for experimental methods that enable rapid and high-resolution characterisation of LLPS phase diagrams. Typically, these are generated by wasteful and laborious methods involving the stepwise and manual combination of reagents to create the requisite variation in solution conditions before observation of individual conditions by microscopy. Notably, although phase diagrams are often used to probe the behaviour of LLPS systems, such experiments can only provide an extremely coarse-grained picture of the protein phase-space when conducted manually.[22,23]

To address this issue, we have devised here a droplet microfluidic approach, termed PhaseScan, that enables rapid, automated generation of different LLPS solution conditions for high-resolution assessment of protein LLPS behaviour. Lab-on-a-chip microfluidic systems, in particular microdroplet-based formats, offer effective means to improve assay throughput, parallelisation, and miniaturisation in biochemical experiments, and have also found recent application in the quantification of protein phase-behaviour on chip.[24–26] However, no technique has yet been demonstrated for the rapid, high-throughput generation of LLPS phase diagrams.

The PhaseScan platform presented herein achieves this objective and allows for the rapid (<3 min) and high-throughput examination of protein LLPS phase behaviour, thereby complementing and expanding upon previous examples of microfluidic investigation of LLPS.[24,27] PhaseScan utilises droplet microfluidics to rapidly generate a large number of compartments, each of which can be considered a discrete microenvironment to study protein LLPS. By altering the input solution conditions, a broad range of phase-separation environments are produced rapidly in order to map LLPS behaviour over a wide region of chemical space.

In our proof-of-concept study, we demonstrate the acquisition of a phase diagram for the G156E mutant of the protein fused in sarcoma (FUS[G156E]), a protein central to the pathology of amyotrophic lateral sclerosis.[9,28] Using our microfluidic platform, we determine the phase boundary between phase-separated and homogeneous FUS solution as modulated by the small molecule 1,6-hexanediol, which is known to strongly interfere with LLPS behaviour, and which has been employed extensively to probe LLPS systems.[17]

Results and Discussion

To implement our platform for high-throughput phase scanning, we first developed a microfluidic droplet generator for the microencapsulation of EGFP-tagged FUS[G156E] under a range of solution conditions (Figure 2a). The device functions by combining the aqueous protein mixture with an immiscible continuous oil phase at a T-junction, which results in the generation of protein-filled water-in-oil microcompartments of ~700 pL volume. The fluorinated oil phase is supplemented with a biologically compatible polyglycerol-based triblock surfactant (see Supporting Information) to prevent droplet coalescence after generation.[29] Prior to the T-junction, buffer, protein, and 1,6-hexanediol solutions are combined in different ratios (Figure 2b, see also Supporting Information) to define the range

of protein and 1,6-hexanediol concentrations scanned by the microfluidic platform. Alexa647 dye (10 μM) is included in the 1,6-hexanediol solution, to provide a fluorescent barcode for the intra-droplet 1,6-hexanediol concentration, whilst the concentration of FUS[G156E] is reported by the intrinsic EGFP tag.

A pre-programmed syringe pump controls the input flow rates of the aqueous droplet components, enabling automated sampling of chemical space (Figure 2b). Laminar flow prevents mixing of the assay components prior to encapsulation, before rapid mixing occurs after droplet generation.[30] Droplets are then collected off-chip under a layer of mineral oil to prevent evaporation. Samples were collected for three minutes, to allow time for a sufficient number of droplets across the full range of conditions to be created, before undergoing fluorescence microscopy imaging analysis (Figure 3a, see also Supporting Information).

To determine the concentration of FUS[G156E] and 1,6-hexanediol present in each droplet, as well as the presence or absence of protein phase separation, fluorescence images underwent automated image analysis using a Python script (Figure 3a,b). Droplet outlines were found by fluorescence thresholding, before the volume-normalised EGFP and Alexa647 fluorescence present in each droplet was quantified. Phase separation was determined by the presence of discrete puncta in EGFP fluorescence, corresponding to phase separated droplets, whereas homogeneous fluorescence indicated the absence of phase separation (Figure 3b).

By combining the measured concentration of droplet FUS[G156E] and 1,6-hexanediol concentration with the presence or absence of phase separation, a phase diagram for the FUS[G156E]/1,6-hexanediol system could be generated (Figure 3c). 1,6-hexanediol is known to strongly inhibit the formation of protein condensates;[17] hence, as expected, phase separation was observable only at low (< 1% (v/v)) concentrations of 1,6-hexanediol, with FUS[G156E] exhibiting a homogeneous phase at higher alcohol concentrations. Over the FUS[G156E] concentrations surveyed (0.95–7.67 μM), the observed phase boundary has only a small gradient which we attribute to concomitant variation in KCl salt concentration (7–56 mM) with that of the protein, due to on-chip dilution of the protein stock solution (167 mM KCl, see Supporting Information).

With information on the phase diagram, and specifically the phase boundary between the demixed and phase-separated state, we utilised Flory–Huggins theory[31–33] to extract further thermodynamic information. Flory–Huggins theory is a commonly employed lattice model for the characterisation of polymer phase behaviour, which describes the free energy of polymer

mixing/demixing $(\frac{f}{k_B T})$ according to the volume fraction (Φ) of the constituent solution components; the model is also dependent on the number of lattice sites N in which molecules are about to interact. We used a simplified three‑component Flory–Huggins equation[33,34] with FUS, 1,6-hexanediol (hex), and the buffer as the constituent solution components, in which each of the components have pairwise interaction parameters χ according to:

$$\frac{f}{k_B T} = (\frac{\Phi_{FUS}}{N_{FUS}} \ln \Phi_{FUS} + \frac{\Phi_{hex}}{N_{hex}} \ln \Phi_{hex} + \Phi_{buffer} \ln \Phi_{buffer}) +$$
$$\chi_{FUS, hex} \Phi_{FUS} \Phi_{hex} + \chi_{FUS, buffer} \Phi_{FUS} \Phi_{buffer} + \chi_{hex, buffer} \Phi_{hex} \Phi_{buffer} \qquad (1)$$

In Equation 1, the first line relates the entropic contributions to phase separation or mixing, and the second line informs on the corresponding enthalpic contributions. For lattice sites we used $N_{FUS} = 526$, representing the number of amino acid residues of FUS^{G156E}, and $N_{hex} = 2$ for each of the hydroxyl groups on the molecule. We utilised known constraints on χ-values to constrain the fit, such as $\chi_{FUS, buffer} > 0$, since FUS is driven to phase separate when alone in buffer, and $\chi_{FUS, hex}$, $\chi_{hex, buffer} < 0$, as 1,6-hexanediol alone dissolves FUS and since the diol is soluble in buffer. Using this simplified three‑component Flory–Huggins framework, we were able to determine an estimate for the free-energy landscape of the phase separation process (Figure 3d), and obtain estimates for the enthalpic (H_{mix}) and entropic (S_{mix}) contributions to the overall free energy of mixing (Figure 3d, inset). These findings exemplify the rapid extraction of data pertaining to the thermodynamics of the LLPS system by our microfluidic platform, and we predict that measurement of mixing enthalpies and entropies in this manner will enable facile mechanistic insights into the effect of external modulators and solution conditions on phase separation behaviour.

Our approach thus enables not only determination of the position of the phase-boundary with significantly improved resolution in terms of solution conditions, relative to manual experiments, but also allows the extraction of free-energy parameters. It therefore shows great potential for *in vitro* characterisation of LLPS thermodynamics, and for the investigation of factors such as sequence variations and mutations, the presence of interfering small molecules, or coacervating polymers such as nucleic acids or other protein species that affect the position of phase equilibria.

Conclusion

Using our microfluidics-based PhaseScan approach, the position of the LLPS phase-boundary for FUS^{G156E} in the presence of 1,6-hexandiol was mapped, and a thermodynamic characterisation of the system was performed, following the generation and assay of >250 independent measurements within five minutes (3 minutes droplet generation, 2 minutes imaging time). This assay throughput is significantly greater than that achievable by manual or previously reported microfluidics experiments, with the subsequent increase in the number of data points enabling an improved fitting of the position of the protein phase boundary. Hence, the PhaseScan platform allows examination of LLPS phase behaviour with unprecedented speed and throughput.

Our study thus provides a basis for the rapid acquisition of LLPS phase diagrams through the application of microdroplet techniques. We note that with the droplet generation rate we observe here (~30 Hz), future experiments could achieve an improved assay throughput by integrating the droplet-microscopy step with droplet generation. In addition, the droplet generation rate can be increased to improve throughput further. In this manner, it is feasible that phase diagrams can be acquired on the order of seconds, rather than minutes. We envisage that microfluidic platforms such as those presented here can find many applications in the quantitation of LLPS equilibria, such as, for example, the screening of candidate small molecules for the therapeutic modulation of phase-separation behaviour.

Acknowledgements

Conflict of interest

Parts of this work have been the subject of a patent application filed by Cambridge Enterprise Limited, a fully owned subsidiary of the University of Cambridge.

References

1. Boeynaems, S. *et al.* Protein Phase Separation: A New Phase in Cell Biology. *Trends Cell Biol.* **28**, 420–435 (2018).

2. Hyman, A. A., Weber, C. A. & Jülicher, F. Liquid-Liquid Phase Separation in Biology. *Annu. Rev. Cell Dev. Biol.* **30**, 39–58 (2014).

3. Shin, Y. & Brangwynne, C. P. Liquid Phase Condensation in Cell Physiology and Disease. *Science* **357**, (2017).

4. Banani, S. F., Lee, H. O., Hyman, A. A. & Rosen, M. K. Biomolecular condensates: Organizers of cellular biochemistry. *Nature Reviews Molecular Cell Biology* **18**, 285–298 (2017).

5. Sokolova, E. *et al.* Enhanced transcription rates in membrane-free protocells formed by coacervation of cell lysate. *Proc. Natl. Acad. Sci. U. S. A.* **110**, 11692–11697 (2013).

6. Kim, T. H. *et al.* Phospho-dependent phase separation of FMRP and CAPRIN1 recapitulates regulation of translation and deadenylation. *Science* **365**, 825–829 (2019).

7. Riback, J. A. *et al.* Stress-Triggered Phase Separation Is an Adaptive, Evolutionarily Tuned Response. *Cell* **168**, 1028-1040.e19 (2017).

8. Boeynaems, S. *et al.* Phase Separation of C9orf72 Dipeptide Repeats Perturbs Stress Granule Dynamics. *Mol. Cell* **65**, 1044-1055.e5 (2017).

9. Patel, A. *et al.* A Liquid-to-Solid Phase Transition of the ALS Protein FUS Accelerated by Disease Mutation. *Cell* **162**, 1066–1077 (2015).

10. Bouchard, J. J. *et al.* Cancer Mutations of the Tumor Suppressor SPOP Disrupt the Formation of Active, Phase-Separated Compartments. *Mol. Cell* **72**, 19-36.e8 (2018).

11. Mullard, A. Biomolecular condensates pique drug discovery curiosity. *Nat. Rev. Drug Discov.* (2019). doi:10.1038/d41573-019-00069-w

12. Wheeler, R. J. *et al.* Small molecules for modulating protein driven liquid-liquid phase

separation in treating neurodegenerative disease. *bioRxiv* 721001 (2019). doi:10.1101/721001

13. Li, Q. *et al.* LLPSDB: a database of proteins undergoing liquid-liquid phase separation in vitro. *Nucleic Acids Res.* **48**, D320–D327 (2020).

14. Alberti, S., Gladfelter, A. & Mittag, T. Considerations and Challenges in Studying Liquid-Liquid Phase Separation and Biomolecular Condensates. *Cell* **176**, 419–434 (2019).

15. Riback, J. A. *et al.* Composition-dependent thermodynamics of intracellular phase separation. *Nature* **581**, 209–214 (2020).

16. Braun, M. K. *et al.* Reentrant Phase Behavior in Protein Solutions Induced by Multivalent Salts: Strong Effect of Anions Cl - Versus NO 3-. *J. Phys. Chem. B* (2018). doi:10.1021/acs.jpcb.8b10268

17. Kroschwald, S., Maharana, S. & Simon, A. Hexanediol: a chemical probe to investigate the material properties of membrane-less compartments. *Matters* (2017). doi:10.19185/matters.201702000010

18. Wheeler, R. J. Therapeutics—How to Treat Phase Separation-Associated Diseases. *Emerg. Top. Life Sci.* (2020). doi:10.1042/ETLS20190176

19. Alberti, S. & Dormann, D. Liquid–Liquid Phase Separation in Disease. *Annu. Rev. Genet.* **53**, 171–194 (2019).

20. Klamser, J. U., Kapfer, S. C. & Krauth, W. Thermodynamic phases in two-dimensional active matter. *Nat. Commun.* **9**, 5045 (2018).

21. Bracha, D. *et al.* Mapping Local and Global Liquid Phase Behavior in Living Cells Using Photo-Oligomerizable Seeds. *Cell* **175**, 1467-1480.e13 (2018).

22. Yang, P. *et al.* G3BP1 Is a Tunable Switch that Triggers Phase Separation to Assemble Stress Granules. *Cell* **181**, 325-345.e28 (2020).

23. Peskett, T. R. *et al.* A Liquid to Solid Phase Transition Underlying Pathological Huntingtin Exon1 Aggregation. *Mol. Cell* **70**, 588-601.e6 (2018).

24. Kopp, M. R. G. *et al.* Microfluidic Shrinking Droplet Concentrator for Analyte Detection and Phase Separation of Protein Solutions. *Anal. Chem.* **92**, 5803–5812 (2020).

25.   Taylor, N. *et al.* Biophysical characterization of organelle-based RNA/protein liquid phases using microfluidics. *Soft Matter* **12**, 9142–9150 (2016).

26.   Celetti, G. *et al.* The liquid state of FG-nucleoporins mimics permeability barrier properties of nuclear pore complexes. *J. Cell Biol.* **219**, e201907157 (2020).

27.   Linsenmeier, M. *et al.* Dynamics of Synthetic Membraneless Organelles in Microfluidic Droplets. *Angew. Chemie Int. Ed.* **58**, 14489–14494 (2019).

28.   van Blitterswijk Marka; Landers, J. E. RNA processing pathways in amyotrophic lateral sclerosis. *Neurogenetics* **11**, 275–290 (2010).

29.   Agresti, J. J. *et al.* Ultrahigh-throughput screening in drop-based microfluidics for directed evolution. *Proc. Natl. Acad. Sci. U. S. A.* **107**, 4004–9 (2010).

30.   Song, H., Tice, J. D. & Ismagilov, R. F. A microfluidic system for controlling reaction networks in time. *Angew. Chemie - Int. Ed.* **42**, 768–772 (2003).

31.   Flory, P. J. Thermodynamics of High Polymer Solutions. *J. Chem. Phys.* **10**, 51–61 (1942).

32.   Brangwynne, C. P., Tompa, P. & Pappu, R. V. Polymer physics of intracellular phase transitions. *Nat. Phys.* **11**, 899–904 (2015).

33.   Lee, C. F., Brangwynne, C. P., Gharakhani, J., Hyman, A. A. & Jülicher, F. Spatial Organization of the Cell Cytoplasm by Position-Dependent Phase Separation. *Phys. Rev. Lett.* **111**, 088101 (2013).

34.   Brady, J. P. *et al.* Structural and hydrodynamic properties of an intrinsically disordered region of a germ cell-specific protein on phase separation. *Proc. Natl. Acad. Sci.* **114**, E8194–E8203 (2017).
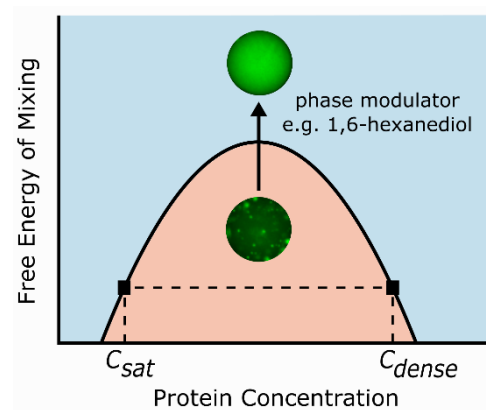
Figures

Figure 1. Liquid–liquid phase separation of protein solutions occurs when the free energy of the system is lowered by partition of proteins from homogeneous solution into a condensed, protein-rich phase and a dilute, protein-depleted phase. Modulators such as 1,6-hexanediol affect the protein free energy of mixing, which can cause the system to transition from the phase-separated to the homogeneous state. c_{sat} and c_{dense} are the saturation concentration, corresponding to the concentration of the dilute phase, and concentration of the condensed phase, respectively.
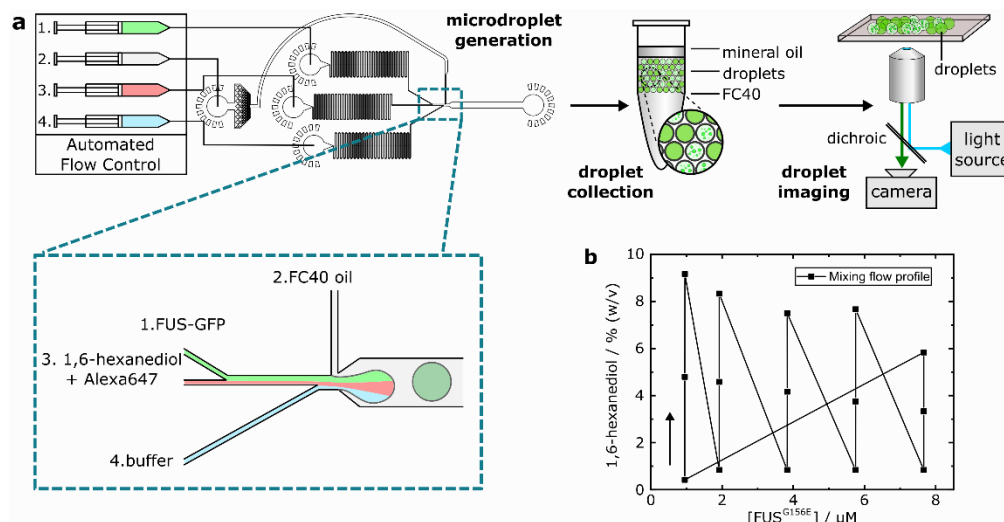
Figure 2. Schematic of the PhaseScan platform and the experimental workflow. **(a)** Droplets are generated using a microfluidic device controlled by automated syringe pumps. Combination of aqueous droplet components prior to the droplet-generating junction (inset) enables variation in droplet solution composition. Droplets are collected off-chip, before undergoing analysis by epifluorescence microscopy. **(b)** Set points for FUS[G156E] and 1,6-hexanediol concentrations as produced by automated flow control in droplet generation (see Supporting Information). The arrow indicates the beginning of the continuous flow programme loop.
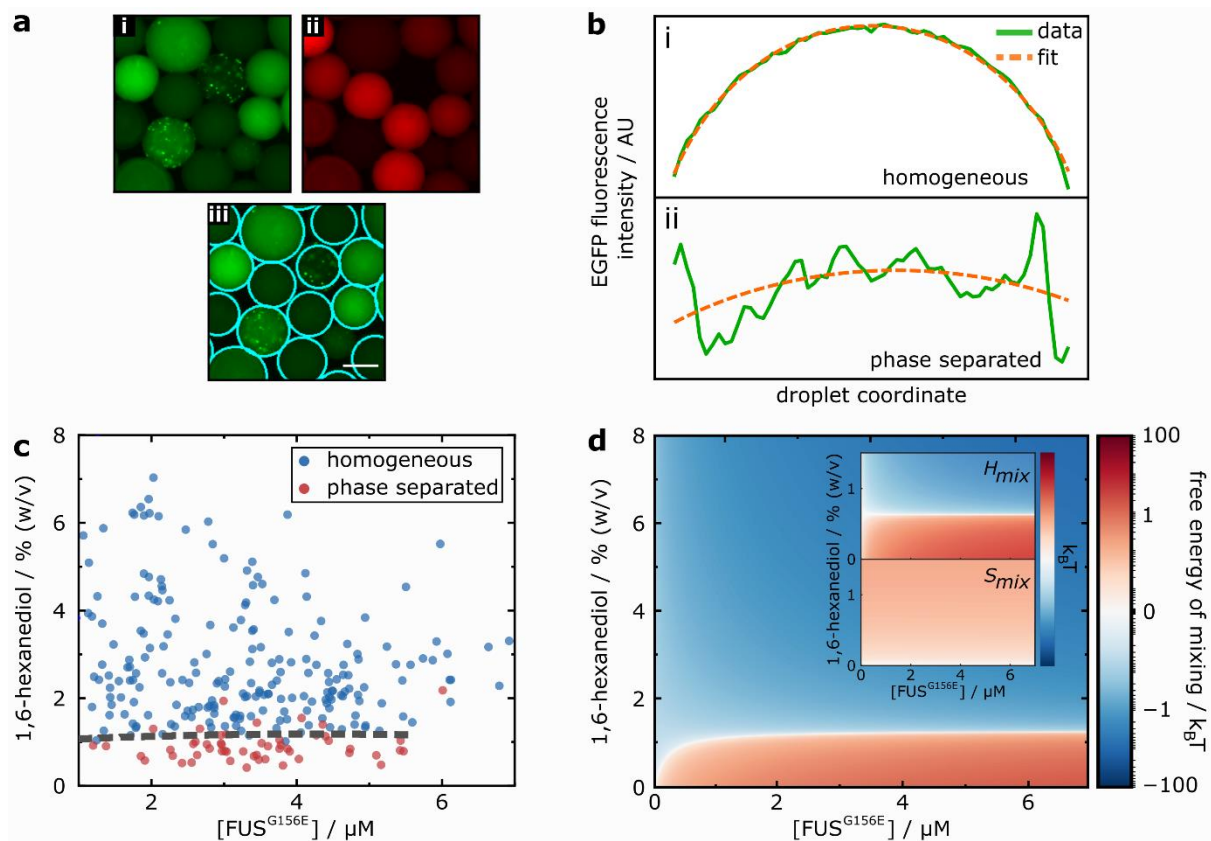
Figure 3. (a) Epifluorescence microscopy images of oil-in-water droplets containing various concentrations of (i) EGFP-labelled FUS[G156E] and (ii) 1,6-hexanediol, with the concentration of the latter indicated by fluorescence of co-encapsulated Alexa647. (iii) Output of automated droplet edge-detection. **(b)** Determination of the presence or absence of intra-droplet phase separation. (i) A close fit of a Gaussian curve (dashed orange lines) to a 1D-projection of droplet EGFP fluorescence (solid green lines) indicates a homogeneous droplet, whilst (ii) a poor fit indicated phase separation. **(c)** Phase diagram for FUS[G156E] as function of protein and 1,6-hexanediol concentration. Points represent measured solution conditions for individual microdroplets ($N = 266$), with presence or absence of phase-separation indicated by blue or red colouring, respectively. Dashed line is a fit generated by a support-vector machine algorithm for classification of the boundary between homogeneous and phase-separated droplet populations (see Supporting Information). **(d)** Estimate of the free-energy landscape for the FUS[G156E]/1,6-hexanediol system, according to the apparent phase boundary (dashed line) in (c). Free energy is reported in terms of the thermal energy k_BT. (Inset) Enthalpic (H_{mix}) and entropic (S_{mix}) contributions to overall free energy of mixing. Colour scale is plotted using same axis as in main figure.